Journal of Sciences, Islamic Republic of Iran 31(4): 337 - 348 (2020) http://jsciences.ut.ac.ir
University of Tehran, ISSN 1016-1104

Spatial Data and Remote Sensing Techniques Integration to Detection and Slicing of Bavanat Red Bed Copper Deposits (NE Shiraz, Iran)

K. Noori Khankahdani*

Department of Geology, Shiraz Branch, Islamic Azad University, Shiraz, Islamic Republic of Iran

Received: 23 October 2019 / Revised: 18 August 2020 / Accepted: 14 September 2020

Abstract

Bavanat red bed copper deposits (Jolani area) are located in south Sanandaj-Sirjan metamorphic belt and approximately 15 km NW of Bavanat. In terms of lithology, these deposits include purple to red siltstone(PSS) which are also seen among the layers of green sandstone(GS). Copper mineralization such as malachite is observed in the GS unit at the surface. Both PSS and GS units have Jurassic age. The current study, has used Landsat 8 and SPOT 5 images for RS processing. This study indicated that RGB=432 color composite in SPOT 5 image has the best contrast for enhancement and detection of PSS and GS units. Only the Landsat 8 fused image has been able to enhance and detect the GS unit. Also, based on band ratio technique, RGB=(b6/b2), (b5/b3), (b7/b1) color composite for Landsat 8 data, has the best contrast for PSS and GS units. PCA method shows that RGB=PC4, PC2, PC1 for Spot 5 data and RGB=PC1, PC2, PC3 for Landsat 8 data have the best contrast for enhancement and detection of the Bavanat red bed copper deposits. In this study, different methods of supervised classification such as SAM, SID and SVM were reviewed. Among these methods, SVM technique has the best layout for SPOT 5 image. This important layout as a basic geological map, can be very useful in additional exploration studies on the Bavanat red bed deposits.

Keywords: Bavanat; Red Bed Copper Deposits; Spatial and RS Data.

Introduction

Red bed copper deposits, are an important group of sedimentary copper deposits that introduced by Emmons [1] for first time. In red bed deposits, the host rock can be concordant or interbedded layers with red, purple and violet sandstone, siltstone or conglomerate formed in deltaic, river or aeolian origin environments [2]. Red bed copper deposits, have been studied in different parts of the world. One of the most famous deposits, is Nacimiento deposit in USA, that have been studied by various scholars including Woodward et al., [3], Talbott [4], Kirkham [5], and Cox et al., [2]. Also, these sedimentary copper deposits have been introduced in Iran for example by Aghazadeh and Badrzadeh [6], Noori Khankahdani and Karimi [7], Karimi [8], Hassanpour and Senemari [9], Sadati et al., [10], Azaraien et al., [11], Rajabpour et al., [12] and Noori Khankahdani and Karimi [13]. The use of remote

* Corresponding author: Tel:09177125196; Fax: +7136410059; Email: noorikamal@yahoo.com

sensing techniques in detection and slicing of mineral deposits results in saving time and money, as well as increase in the accuracy of the operation, therefore, it has been considered by many researchers. The purpose of such techniques is to integrate field and RS data using more accurate digital methods to perform the enhancement, detection and slicing of various units [14]. Several researchers have used remote sensing techniques in order to detect and explore mineral resources. For example, Noori Khankahdani and Zarei, [15], Honarmand et al., [16], Pour and Hashim, [17], Hosseinjani Zadeh et al., [18], Alimohammadi et al., [19] and Rajendran and Nasir, [20]. Due to the spatial expansion of the red bed copper deposits in the Bavanat area, simultaneous use of field data and remote sensing techniques can be very beneficial for detection and slicing of these deposits. In current study, this combination was done and the results were quite satisfactory.

The Geological Environment

According to Mohajjel and Fergusson [21], Bavanat area is located in south section of Sanandaj-Sirjan metamorphic zone (Fig. 1). An impotent lithological

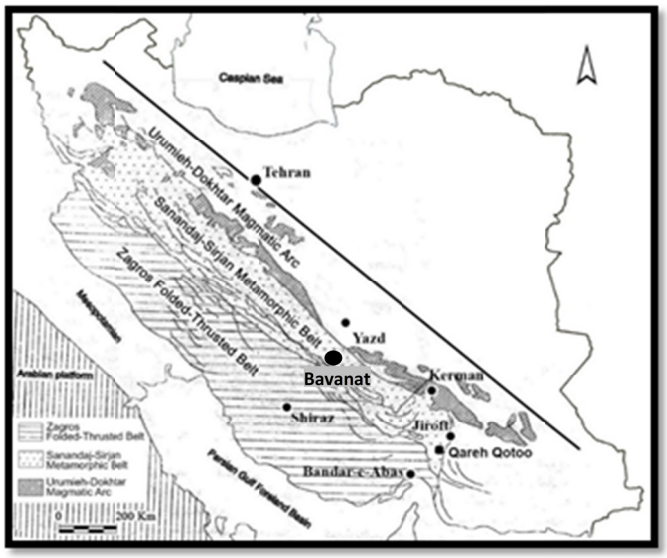

Figure 1. The location of Bavanat study area in Sanandaj-Sirjan metamorphic belt (base map from Mohajjel and Fergusson, 2000).

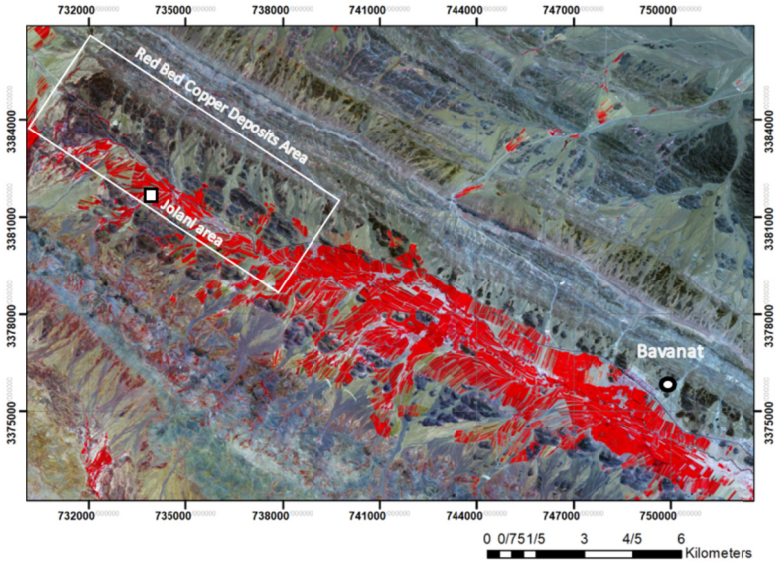

Figure 2. Location of the red bed copper deposits in the Jolani region, 15 km NW of Bavanat.

unit outcropped in N-NW section of Bavanat valley which is especially important in terms of copper mineralization (Fig. 2). This unit includes purple to red siltstone (PSS) with Jurassic age and has interbeds of green sandstone (Fig. 3 and Fig. 4). In fact, copper mineralization is observed in the exact same green sandstone unit. Previous studies by Noori Khankahdani and Karimi [7], Vahid [22]], Chaman Ara [23], and Noori Khankahdani and Karimi [13] have shown these copper deposits are placed in red bed copper deposits.

Figure 5 shows hand sample and microscopic images of PSS and GS (green sandstone) units. Copper

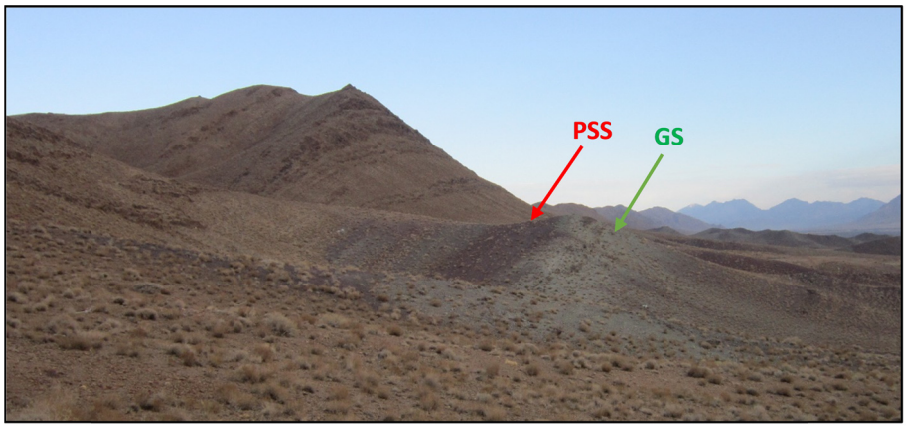

Figure 3. The outcrop of purple siltstone(PSS) and green sandstone(GS), View to NE, These lithological units, form Bavanat red bed copper deposits.

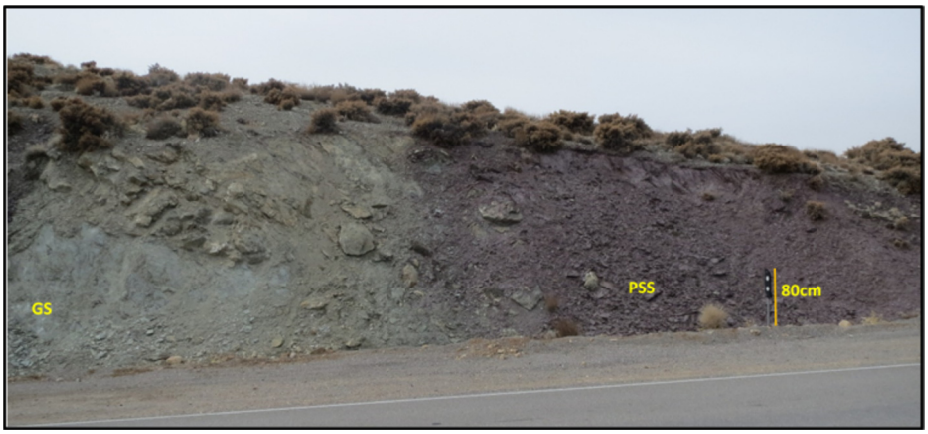

Figure 4. Close up image of PSS and GS units (Bavanat red bed copper deposit) Dehbid-Bavanat road.

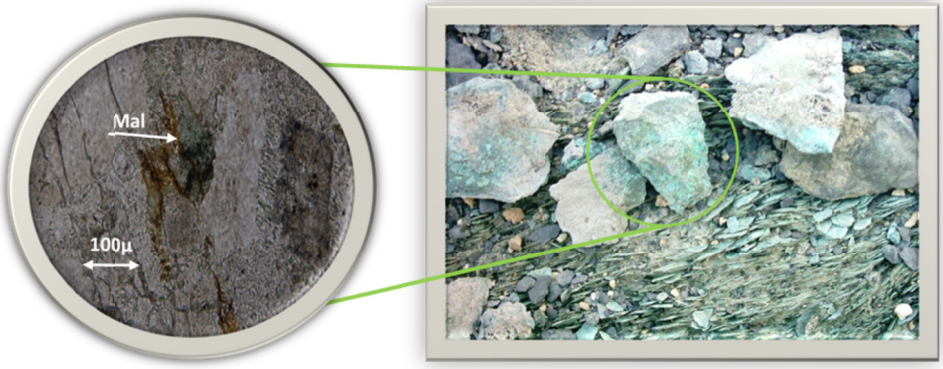

Figure 5. Copper mineralization as malachite in macroscopic(right) and microscopic scale(left).

Table 1. Results of XRF chemical analysis of Cu-bearing green sandstone (Bavanat area) (Noori Khankahdani and Karimi, 2019).

Sample	SiO_2	Al_2O_3	Fe_2O_3	CaO	MgO	Na_2O	K_2O	P_2O_5	TiO_2	MnO	SO_3	Cu	L.O.I
	%	%	%	%	%	%	%	%	%	%	%	ppm	%
T1S5	69.74	4.11	3.75	10.9	0.5	0.38	0.62	0.042	0.25	0.43	0	91	8.97
T1S6	56.58	20.73	8.15	1.35	2.72	0.66	4.31	0.126	0.78	0.01	0	18	4.16
T1S12	73.85	7.73	2.27	5.21	0.98	2.2	0.4	0.047	0.21	0.21	0	12826	5.19
T1S13	72.8	8.82	6.48	1.4	2.51	0.75	0.58	0.071	0.25	0.15	0	17797	3.91
MS18	75.86	9.47	4.73	1.29	2.04	1.13	0.73	0.069	0.29	0.12	0	5477	3.43

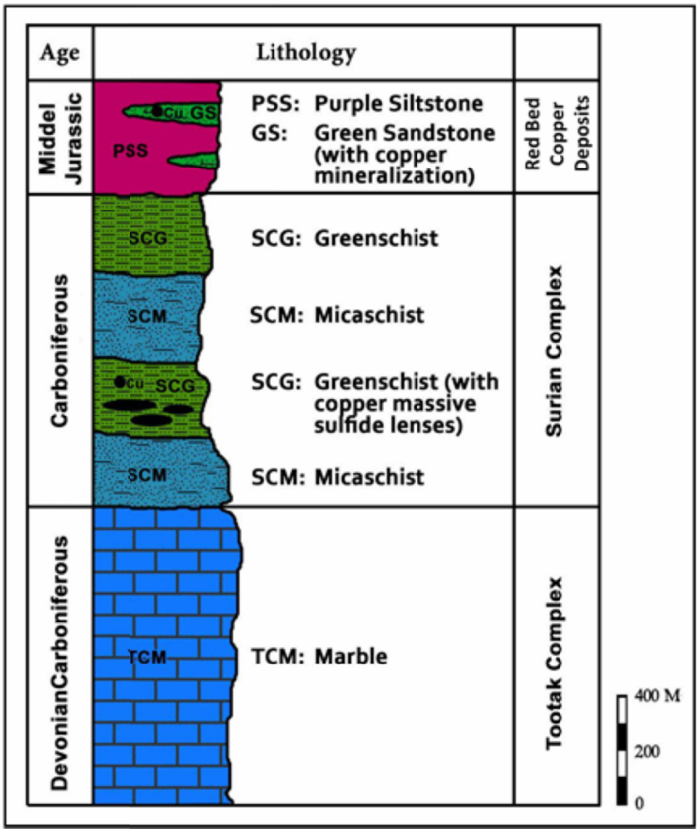

Figure 6. Stratigraphic column of Bavanat red bed copper deposit, Noori Khankahdani and Karimi (2019).

mineralization in GS sample is in the form of Malachite (CuCO3 (OH) 2). Table 1 has shown the results of chemical analysis of a number of Cu-bearing green sandstones in Bavanat region. These analyzes have been performed in Kansaran Binalood company. Also, Figure 6 shows the stratigraphic column of the study area based on Noori Khankahdani and Karimi studies [13]. The main purpose of current studies is enhancement, detection and slicing of PSS and GS units so that further exploration can be focused on.

Materials and Methods

In this research, field areas of the purple siltstone (PSS) and green sandstones (GS) were studied first. Table 2 shows the geographical coordinates of the PSS and GS points. These points have been registered at the WGS84 datum. Also, the position of these points is shown on the SPOT 5 image (Fig. 7). The rock samples have been studied in Shiraz Islamic Azad University using a polarizing microscope. After field observations and preliminary identification of PSS and GS units in microscopic studies, Landsat 8 image with row and path

Table 2. The geographical coordinates of the PSS and GS points.

Row	X	Y	Type	Row	X	Y	Type
1	732661	3383414	GS	19	731506	3384634	GS
2	733056	3383357	GS	20	733145	3383301	GS
3	734652	3383615	GS	21	732795	3384653	PSS
4	733403	3383126	GS	22	733433	3384407	PSS
5	732695	3383441	GS	23	733631	3384142	PSS
6	733847	3383077	GS	24	734134	3383743	PSS
7	732427	3384804	GS	25	732826	3384788	PSS
8	731631	3385034	GS	26	732296	3385247	PSS
9	732301	3385072	GS	27	732428	3384922	PSS
10	732032	3385159	GS	28	733147	3384369	PSS
١١	732153	3385029	GS	29	734615	3383232	PSS
12	732322	3384482	GS	30	731822	3384168	PSS
13	732533	3384702	GS	31	732852	3383689	PSS
14	734262	3383816	GS	32	732285	3384625	PSS
15	732766	3384306	GS	33	732894	3384544	PSS
16	733681	3382877	GS	34	732894	3384544	PSS
17	734549	3383688	GS	35	733648	3382965	PSS
18	734151	3382599	GS	36	732566	3385038	PSS

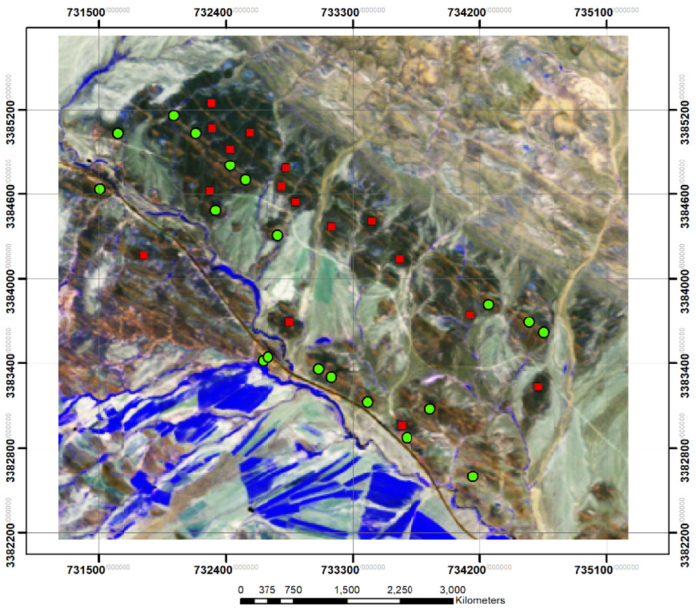

Figure 7. The position of acquired points on SPOT 5 image.
Note: Green Sandstone(GS)=green circle and Purple Siltstone (PSS)=red square.

162-39 (16/09/2018) and SPOT 5 image No. 157-289 (24/08/2005) were utilized for remote sensing operations. For this purpose, ENVI 5.3. software was used. After pre-processing of data, different methods of remote sensing such as construction of color composites, data fusion, band ratio, PCA method and supervised classification were used so that PSS and GS units were detected and separated very well. The results of each section is presented separately as follows.

Results

Color Composites

In order to build the best color composites, at first spectral reflectance curves (Fig. 8) were plotted using ground control points (Table 2). As previous studies have indicated that the most suitable bands to create color composite in one target, are the bands which have the highest reflection for that target [24]. Figure 8 shows spectral reflectance curves for Landsat 8 and SPOT 5.

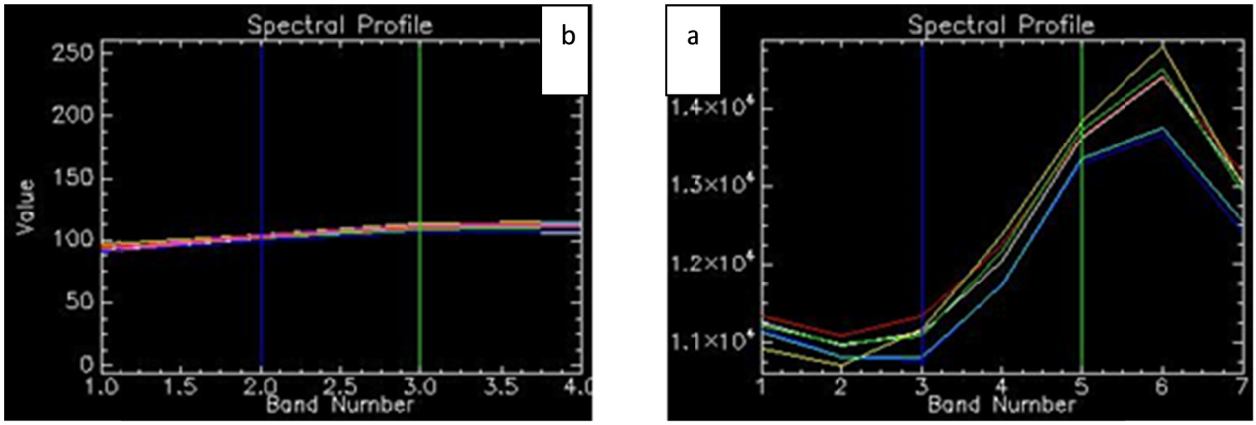

Figure 8. Spectral reflectance curves for PSS unit in Landsat 8.a (right) and SPOT 8.b (left) images.

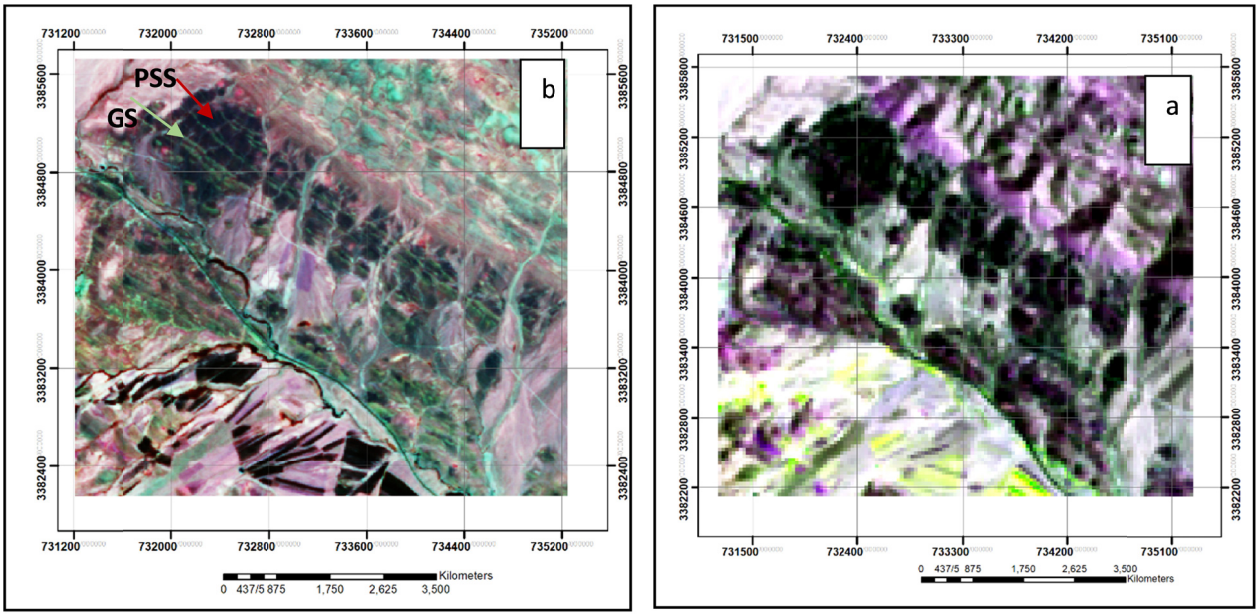

Figure 9. a: (Right). Landsat 8 image(RGB=657), PSS unit is seen in black and is recognized from surrounding units easily, also, in the Landsat 8 image, the GS unit is not visible. B: (Left). SPOT 5 image (RGB=432), PSS unit is seen as black and GS unit appears as green color interbeds inside the PSS unit.

According to Figure 8, for 3 bands of 7,6,5 that have the highest reflectivity in the Landsat 8 image, the following equation is correct:

b6>b5>b7

therefore, RGB=657 will create the best contrast for PSS unit. This argument, has resulted in identifying RGB=432 for SPOT 5. The contrast of PSS unit in false color composites (Fig. 9.a and 9.b) is acceptable and PSS unit can be detected easily.

Data Fusion

Due to spatial resolution of Landsat 8 multispectral bands, enhancement of GS unit is not possible; therefore, pan band of Landsat 8 (b8) was used for data fusion. Gram-Schmidt Pan Sharpening method was used to fuse the Pan images (15 m pixel size) with the 7 multispectral images (30m pixel size) to produce a 15m pixel size [25]. Gram Schmidt Pan-Sharpening method is more accurate than the Principal Component (PC) and Hue, Saturation and Value (HSV) methods because it uses the spectral response function of a given sensor to estimate what the panchromatic data look like. Comparison of a Z Profile of the original image with that of the Gram-Schmidt Pan-Sharpened image revealed that there is no difference in spectral information [26]. Gram Schmidt Pan-Sharpening

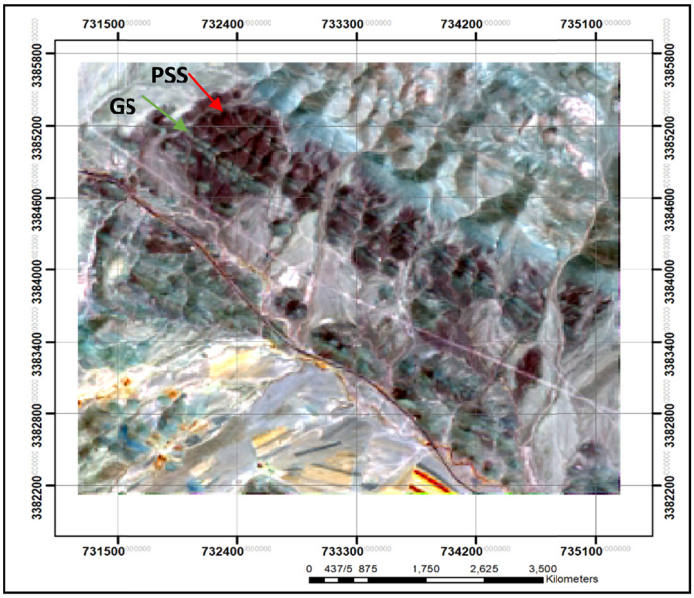

Figure 10. Fused image of Landsat 8, as it is seen fusion technique has created more enhancement of GS unit so as in the above image, PSS and GS units are shown in brown and green colors, respectively.

method is highly recommended for most applications [25]. The result of this technique is completely satisfactory and the GS unit was well enhanced and detected using Landsat 8 fused data (Fig. 10).

Band Ratios

Band ratios is one of the important methods for the rock units enhancement. Image enhancement with band ratio technique is the process implemented for the digital image to produce more interpretable one for a particular application [27]. Enhancement techniques comprises many methods, determined according to the objective, such as Principal Components Analysis (PCA) and Band Ratio, which are significantly helpful

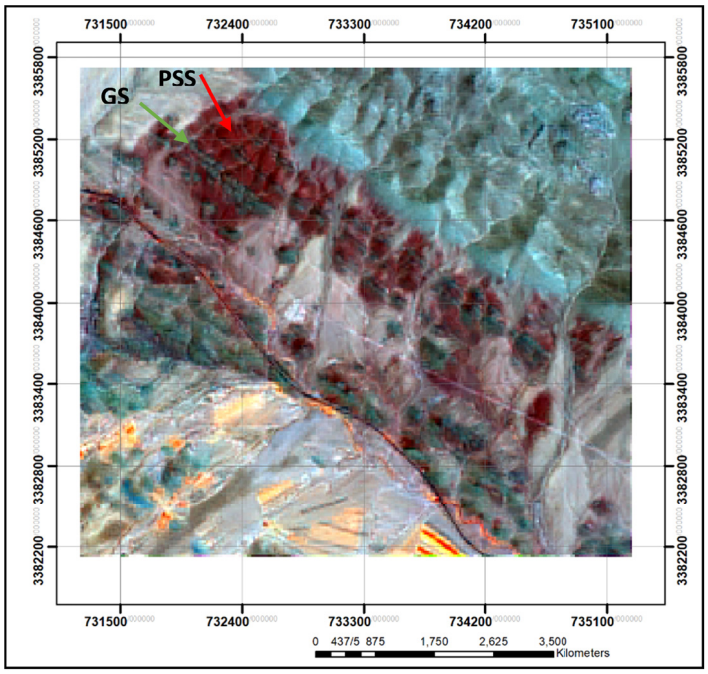

Figure 11. Band ratio image RGB=(b6/b2), (b5/b3), (b7/b1) for Landsat 8, both units (PSS and GS) are detected easily.

in differentiation and recognizing the different rock units, and convolution filtering, which is extremely useful in emphasize the lineation and lineament features as well as geological structures [28]. Bands with the highest and lowest reflection were identified by spectral reflectance curves (Fig. 8.a & 8.b) and have been used in band ratios. For the Landsat 8, 7-band intensity reflections, are as follows as such that b6 shows the highest and b2 the lowest reflection intensity:
b6>b5>b7>b4>b1>b3>b2

Accordingly, the band ratio images of Landsat 8 were created and revealed that the below color composite, has the best contrast for PSS and GS:
RGB=(b6/b2), (b5/b3), (b7/b1)

In the above color composite, the GS unit is green and the PSS unit is purple and both units are identified and differentiated easily (Fig. 11).

PCA Method

The main aim of the principal components analysis (PCA method), is obtaining independent or unrelated indicators in a data set which these data may be are interdependent because non correlation or lowest correlation can reveal their differences [29]. PCA, is a statistical and mathematical method that has a lot of applications for representing differences between satellite images. The most important uses of the PCA method in RS is concentrating and limiting information in a few specified channels and also increasing the amount of information in these channels. In this research, covariance matrix method has been used to calculate PCA, though in PCA technique, one can use both the covariance matrix and the correlation matrix [29]. Figures 12.a and 12.b show PCA images for Landsat 8 and SPOT 5 respectively. As can be seen, PSS and GS units have a very good contrast with their neighboring units which can be very effective in distinguishing it from other rock units.

Supervised Classification

Both images of Landsat 8 and SPOT 5 have been used for supervised classification by SAM, SID and SVM methods. Support Vector Machin(SVM) has a training approach and works through labeling of training samples in the region of interest [30]. This is while the Spectral Angle Mapper (SAM) and Spectral Information Divergence (SID) methods perform based on spectral reflectance curve for one special pixel. Also, previous studies indicated that SAM and SID methods have had good results for the study of alteration zones [26]. Another point is that the SVM method finds a surface that does not only have the most contrast with other surfaces, but also has the smallest error in the output. [31]. The results of supervised classification operations confirm that the output image of the SVM method for SPOT 5 data is the best separation solution for PSS and GS units (Fig. 13). In this operation, the training points are defined for 5 classes which include PSS and GS units in relation with the other 3 defined classes. In the final classification image, the PSS and

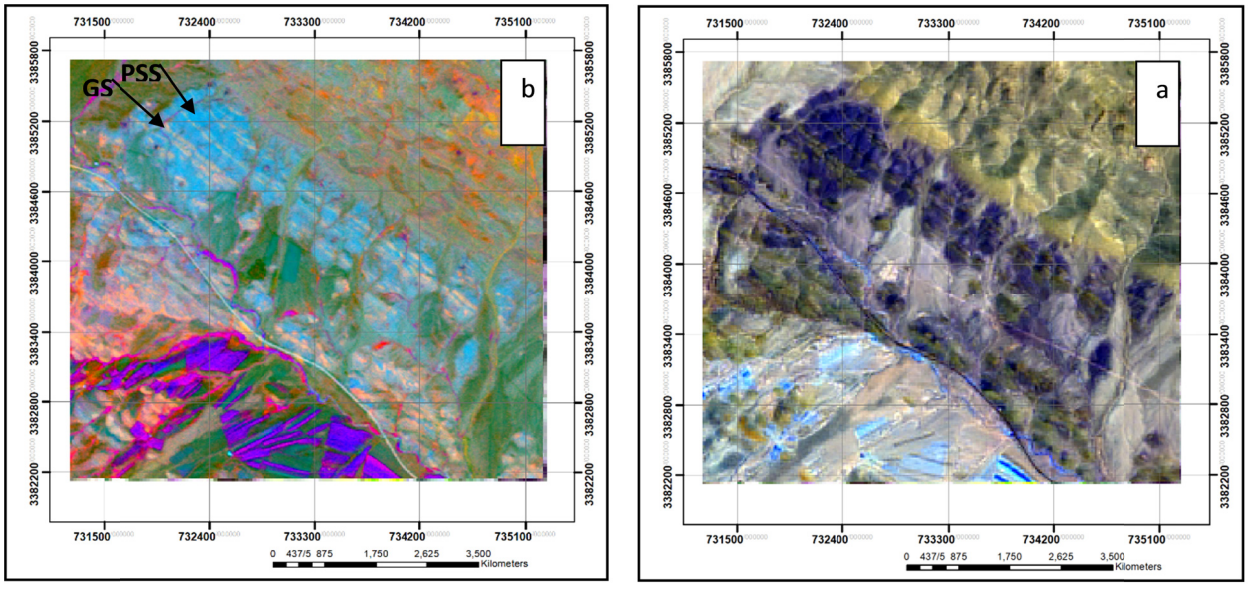

Figure 12. a. RGB=PC1,PC2,PC3 image for Landsat 8 (right), in this image GS unit can be seen in green color and PSS is observed in dark blue color. b. RGB=PC4,PC2,PC1 image for SPOT 5(Left), PSS and GS units are seen respectively in blue and yellow and both have a very good contrast with their neighboring units.

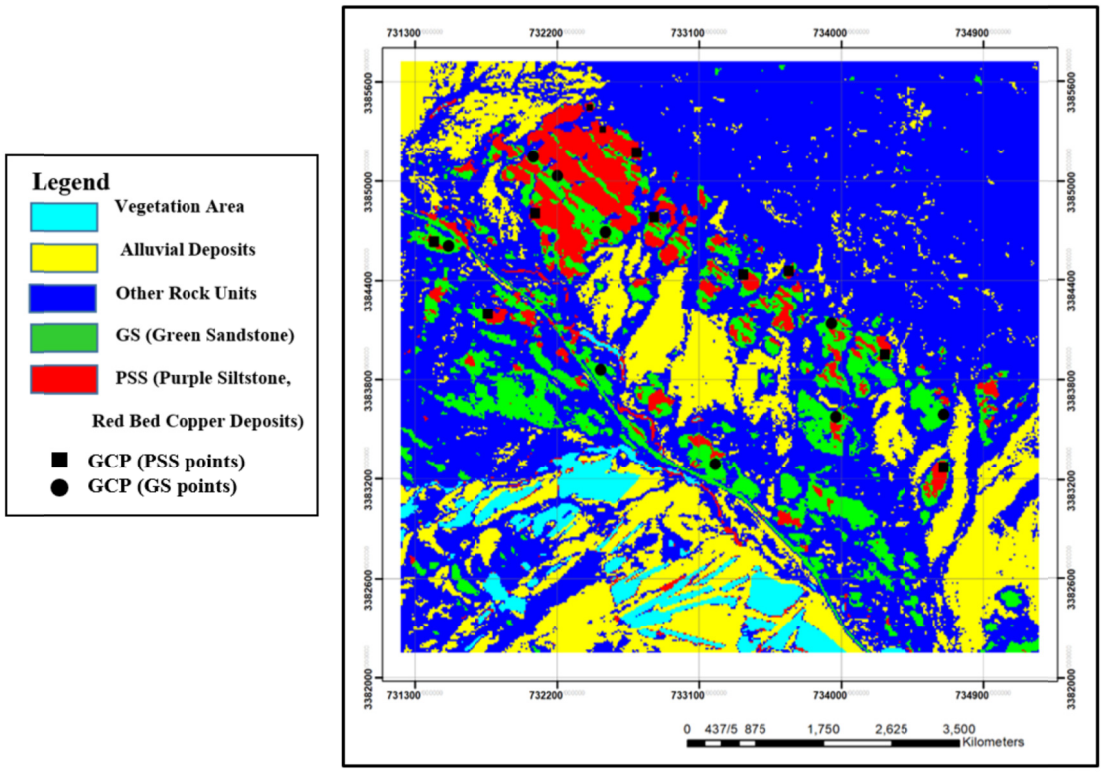

Figure 13. Supervised classification image for Spot 5, in this image, the PSS unit is in red and the GS unit is green, and both units have a very beautiful contrast in relation to other units. The black square for the PSS unit and the black circle for the GS unit are used to represent the ground control points (GCP). This image can be the basis for the preparation of geological maps of this area, especially for the enhancement and detection of the Bavanat red bed copper deposits.

GS units are seen in red and green, respectively and well detectable and separable from surrounding units. The created classification image can be used as a basic geological map in the exploration study for the Bavanat red bed copper deposits. In order to results validation, were used 20 ground control points (Table 3). These points are the results of the field surveys of PSS and GS units which are not used in image processing operations. The review of results validation of satellite image processing in these studies proved the position 19 of 20 ground control points were correctly determined and only the position of 1 point was determined instead of the PSS unit of the GS unit (point No. 10). The cause of this issue has been spectral interference or inaccurate recording of point coordinates. Thus, 95% of the position of points related to PSS and GS units in field studies correspond to the position of these points in satellite image processing (Fig. 13).

Table 3. The geographical coordinates of the Ground Control Points (GCP).

Row	X	Y	Rock Type	Classified rock	Row	X	Y	Rock Type	Classified rock
1	732404	3385447	PSS	PSS	11	734648	3382270	PSS	PSS
2	732485	3385316	PSS	PSS	12	734648	3383590	GS	GS
3	732705	3385174	PSS	PSS	13	733965	3383577	GS	GS
4	732057	3384806	PSS	PSS	14	733937	3384137	GS	GS
5	731760	3384197	PSS	PSS	15	733200	3383288	GS	GS
6	731416	3384636	PSS	PSS	16	732471	3383857	GS	GS
7	732815	3384781	PSS	PSS	17	732503	3384693	GS	GS
8	733378	3384438	PSS	PSS	18	732199	3385032	GS	GS
9	733668	3384459	PSS	PSS	19	731508	3384611	GS	GS
10	734270	3383950	PSS	GS	20	732047	3385149	GS	GS

Discussion

Bavanat red bed copper deposits similar to other known reserves in the world, are important in terms of copper mineralization and other precious elements such as silver and cobalt [5 and 32] and it is necessary to study the area a lot more because the geological data of these rock units still are not fully available. Red bed deposits of this area is called PSS unit and includes interbeds of green sandstones (GS unit). As a matter of fact, copper mineralization has occurred in the GS unit. Walker [33] believes that the reserves of the red layer of the red represents the oxidized zone while the green color indicates the reduction conditions of the sedimentary environment, especially due to the action of organic matters. Also, Hitzman et al., [34] argue that copper mineralization forms on the border between red and green units. The purpose of current study, was enhancement, detection and slicing of PSS and GS units from adjacent units and it confirmed that combining field and remote sensing data can have trustful results for identifying and separating these units. During field studies 38 points from PSS was reviewed and their positions were recorded by GPS. Both microscopic and hand samples studies, proved occurrence of copper mineralization such as malachite in GS unit. Based on RS studies, SPOT 5 data have the ground resolution for enhancement and detection of both PSS and GS units but Landsat 8 is just able to enhance PSS unit. This issue can be related to higher ground resolution of SPOT 5 data compared to Landsat 8 data. Taking this subject into account has led to the use of data fusion techniques which fortunately was effective. These techniques created a high enhancement for GS unit from other units. Also, based on current study, Gram-Schmidt method has had more efficiency compared to other methods for enhancement of GS unit. The use of other techniques such as band ratio and PCA methods has been effective and has brought in more enhancement and detection for PSS and GS units. Band ratios is a general term to describe the processes that combine the pixels of two or more raster layers in mathematical combinations in order to enhance the spectral differences between bands and reduce the effects of topography [28]. In band ratio method, color composite with RGB=(b6/b2), (b5/b3), (b7/b1) has the best contrast for PSS and GS units. But it is interesting to know that this method has no positive results for SPOT 5. The principal component analysis method is generally applied in two approaches: standard and selective formats. In the standard method, all bands are used to construct the components and in fact, the number of bands is equal to the number of principal components (PCs). But in a selective approach some of the bands that demonstrate specific anomalies for the subject matter are selected and component analysis is performed solely on the basis of these bands to increase the probability of highlighting the subject of interest [35]. Between these two methods, the standard PCA method has been more effective in demonstrating PSS and GS units and therefore has been used. Also, RGB=PC4, PC2, PC1 in SPOT 5 and RGB=PC1, PC2, PC3 in Landsat 8 have caused more contrast in the studied units with surrounding units. Various methods of supervised classification have been applied. The basic premise in multi-spectral computer classification is that terrestrial objects possess sufficiently different reflectance properties in different regions of the electromagnetic spectrum [36]. Based on these spectral properties, earth surface features can be discriminated and create a new output image with a specific number of classes or categories [37]. The result of all of these studies illustrated that among the SAM, SID and SVM methods, support vector machine(SVM) has the best performance in detection and slicing of PSS and GS units therefore, this supervised classification method is recommended for other areas with similar conditions. Results validation was confirmed in 95% of ground control points, this issue indicates the classification image which prepared in these studies has a high accuracy for future research.The classification image created in these studies, can be used as a basic geological map in the exploration studies for copper mineralization and other precious elements in Bavanat red bed deposits.

Conclusions

In current studies, simultaneous use of field and remote sensing data has been effective in enhancement, detection and slicing of Bavanat Redbed copper deposits and led to the provision of a basic geological map of these reserves (Fig. 13). This map can be used in future supplementary studies as so all green points on figure 13 can be considered as a point with copper mineralization potential. Furthermore, although the Redbed deposits are mainly important in terms of copper mineralization, they contain other valuable elements such as silver and cobalt as a byproduct. As a result, the supplementary studies model of Bavanat area can be changed from a single-dimensional to a multi-dimensional model so that examine more mineralizations along with copper mineralization in the area.

References

1. Emmons S. F. Copper in the red beds of the Colorado Plateau region. *Bull. U.S. Geol. Surv*. **260:** 221-232 (1905).
2. Cox D. P., Lindsey D. A., Singer D. A. and Diggles M. F. Sediment hosted copper deposits of the world, deposit models and database. *US Geol. Survey,* Open-file report 03-107, P.50 (2007).
3. Woodward L. A., Kaufman W. H., Schumacher O. L. and Talbott L. W. Strata-bound copper deposits in Triassic sandstone of Sierra Nacimiento, Mew Mexico. *Econ. Geol.*,**69:** 108-120 (1974).
4. Talbott L. W. Geology of the Nacimiento mine, New Mexico. *New Mex. Geol. Soc*. 25th Ann. Fld. Conf. Guidebook to Ghost Ranch Region (1974).
5. Kirkham R. V. Distribution, settings and genesis of sediment-hosted stratiform copper deposits in Boyle sediment-hosted stratiform copper deposits. *GAC., Special Paper*, **36**: 3-38 (1989).
6. Aghazadeh M. and Badrzadeh Z. The presence of sedimentary copper mineralization horizons in Iran. *29th Earth Science Conference ,GSI ,Tehran,Iran* (2010).
7. Noori Khankahdani K. and Karimi M. Mineralogical and geochemical studies of copper mineralization in the Surian metamorphic complex (Bavanat, Fars). *Islamic Azad University-Shiraz Branch, research assistant domain* (2013).
8. Karimi M. Mineralogy, geochemistry and genesis of Chehrabad Cu-Pb deposit(Zanjan province). *Geoch.*, **4(1**): 21-36 (2015).
9. Hassanpour Sh. and Senemari S. Mineralogy and Geochemistry Studies of the Sorkheh Sediment-hosted Stratiform Copper (SSC) Deposit, NW Iran. *I.J.E.S.,* **7**: 89-105 (2015).
10. Sadati N., Yazdi M., Mao J., Behzadi M., Adabi M.H., Lingang X., Zhenyu Ch. and Mokhtari M.A.A. Sulfide mineral chemistry investigation of sediment-hosted stratiform copper deposits, Nahand-Ivand area, NW Iran. *ORE. GEOL. REV.,* **72**: 760-776 (2016).
11. Azaraien H., Shahabpour J. and Aminzadeh B. Metallogenesis of the sediment-hosted stratiform Cu deposits of the Ravar Copper Belt(RCB), Central Iran. *ORE. GEOL. REV.,* **81**: 369-396 (2017).
12. Rajabpour Sh., Abedini A., Alipour S., Lehmann B. and Jiang Sh. Geology and geochemistry of the sediment-hosted Cheshmeh-Konan Redbed-type copper deposit, NW Iran. *ORE. GEOL. REV.,* **86**: 154-171 (2017).
13. Noori Khankahdani K. and Karimi M. Sediment-Hosted Copper Mineralization in Bavanat Region, Southern Sanandaj-Sirjan, Iran. *J.Sci.I.R.I.*, **30(1):** 61-75 (2019).
14. Lillesand T.M. and Kiefer R.W. Remote Sensing and Image Interpretation (4th end). New York, John Wiley and Sons (2000).
15. Noori Khankahdani K. and Zarei E. Comparison between standard and selective PCA methods in the enhancement and detection of the dunite of Neyriz ophiolite sequence. *16th Annual Conference, Geological Society of Iran, Shiraz University* (2012).
16. Honarmand M., Ranjbar H. and Shahabpour J. Application of principal component analysis and spectral angle mapper in the mapping of hydrothermal alteration in the Jebal-Barez Area, Southeastern Iran. *Resour Geol.* **62**: 119–139 (2012).
17. Pour A.B. and Hashim M. The application of ASTER remote sensing data to porphyry copper and epithermal gold deposits. *ORE. GEOL. REV.* **44**: 1–9 (2012).
18. Hosseinjani Zadeh M., Tangestani M.H., Roldan F.V. and Yusta I. Spectral characteristics of minerals in alteration zones associated with porphyry copper deposits in the middle part of Kerman copper belt, SE Iran. *ORE. GEOL. REV*. **62**: 191–198 (2014).
19. Alimohammadi M., Alirezaei S. and Kontak D.J. Application of ASTER data for exploration of porphyry copper deposits: a case study of Daraloo-Sarmeshk area, southern part of the Kerman copper belt, Iran. *ORE. GEOL. REV*. **70**: 290–304 (2015).
20. Rajendran S. and Nasir S. Characterization of ASTER spectral bands for mapping of alteration zones of volcanogenic massive sulphide deposits. *ORE GEOL REV.,* **88:** 317–335 (2017).
21. Mohajjel M. and Fergusson Ch. Dextral transpression in Late Cretaceous continental collision, Sanandaj–Sirjan Zone, western Iran. *J. Struct. Geol*, **22: (8)**, 1125-1139 (2000).
22. Vahid P. Economic and genetic estimate of Taher Abad copper deposit, (The east of Bavanat). *MS thesis, Islamic Azad University, Shiraz Branch* (2016).
23. Chaman Ara A.R. The study of Mineralogy, geochemistry and genesis of copper mineralization in the Bavanat region (NE of Fars province) and its relationship with structural elements. *PhD thesis, Islamic Azad University, North Tehran Branch* (2016).
24. Curran P.J. Principles of Remote Sensing. Longman Group Limited, London (1985).
25. Laben C.A. and Brower B.V. Process for Enhancing the Spatial Resolution of Multispectral Imagery using Pan-Sharpening. U.S. Patent, 6, 011, 875 (2000).
26. Amer A. Mezayen A. and Hasanein M. ASTER spectral analysis for alteration minerals associated with gold mineralization. *ORE GEOL REV,* **75**: 239–251 (2016).
27. Faust N.L. Image enhancement. In: Kent, A. Williams, J.G. (Eds.) Supplement 5 of Encyclopedia of Computer Science and Technology. **20**: Marcel Dekker, Inc., New York (1989).
28. Abdelmalik K.W. and Abd-Allah A.M.A. Integration of remote sensing technique and field data in geologic mapping of an ophiolitic suture zone in western Arabian Shield. *J. Afr. Earth Sci.,* **146**: 180-190 (2018)
29. Mather P.M. Computer Processing of Remotely Sensed Images. John Wiley & Sons (1999).
30. Richards J.A. and Jia X. Remote Sensing Digital Image Analysis. Springer-Verlag, Berlin, Fourth Edition (2006).
31. Chapelle O., Vapnik V. and Bengio Y. Semi-Supervised Learning. The MIT Press (2006).
32. Cabral A. R. Red-bed copper deposits of the Quebec Appalachians. *Final results of the research project, Laval University, Quebec* (2006).
33. Walker T.R. Application of diagenetic alterations in redbeds to the origin of copper in stratiform copper deposits. In Sediment-Hosted Stratiform Copper Deposits; Boyle R.W. Brown A.C. Jefferson C.W. Jowett E.C. Kirkham R.V. Eds. Geological Association of Canada

Special Paper. *GAC,* **36**: 85–96 (1989).

34. Hitzman M., Kirkham R., Broughton D., Thorson J. and Selley D. The sediment-hosted stratiform copper ore system. *Eco. Geol.,* **100th Anniversary Volume**, 609-642 (2005).
35. Loughlin W. P. Principal Component Analysis for Alteration Mapping-Photogrammetric. *Eng. and Rem. Sen.*, **57**: 1163-1169 (1991).
36. Kaiser M. F. Aboulela H. EL Serehy H. and Ezz Edin H. Spectral enhancement of SPOT imagery data to assess marine pollution near Port Said, Egypt. *Int. J. Remote Sens.,* **31(7):** 1753–1764 (2010).
37. Singh A. Digital change detection techniques using remotely-sensed data. *Int. J. Remote Sens.,* **10**: 989–1003 (1989).